New Journal of Physics
The open-access journal for physics

Quantum–classical transition in the electron dynamics of thin metal films

R Jasiak[1], G Manfredi[1,3], P-A Hervieux[1] and M Haefele[2]

[1] Institut de Physique et Chimie des Matériaux, CNRS and Université de Strasbourg, BP 43, F-67034 Strasbourg, France

[2] INRIA Nancy Grand-Est and Institut de Recherche en Mathématiques Avancées, 7 rue René Descartes, F-67084 Strasbourg, France

E-mail: Giovanni.Manfredi@ipcms.u-strasbg.fr

New Journal of Physics **11** (2009) 063042 (15pp)
Received 31 March 2009
Published 22 June 2009
Online at http://www.njp.org/
doi:10.1088/1367-2630/11/6/063042

Abstract. The quantum electrons dynamics in a thin metal film is studied numerically using the self-consistent Wigner–Poisson equations. The initial equilibrium is computed from the Kohn–Sham equations at finite temperature, and then mapped into the phase-space Wigner function. The time-dependent results are compared systematically with those obtained previously with a classical approach (Vlasov–Poisson equations). It is found that, for large excitations, the quantum and classical dynamics display the same low-frequency oscillations due to ballistic electrons bouncing back and forth on the film surfaces. However, below a certain excitation energy (roughly corresponding to one quantum of plasmon energy $\hbar\omega_p$), the quantum and classical results diverge, and the ballistic oscillations are no longer observed. These results provide an example of a quantum–classical transition that may be observed with current pump–probe experiments on thin metal films.

[3] Author to whom any correspondence should be addressed.

Contents

1. Introduction

The last few decades have witnessed a dramatic development of ultrafast spectroscopy techniques. Femtosecond laser pulses are now routinely utilized in the laboratory to probe the electron dynamics in metallic nanostructures, while sub-femtosecond (attosecond) spectroscopy is rapidly developing.

The typical experimental setup is that of a 'pump–probe' experiment: the system is perturbed via a first stronger laser pulse (the pump), followed by a second weaker pulse (the probe) that acts as a diagnostic tool. By modulating the relative amplitude of the signals, as well as the delay between the pump and the probe, it is possible to assess with great precision the dynamical relaxation of the electron gas [1]–[5].

The possibility to study the electron dynamics on such short timescales has opened new interesting avenues for research, both fundamental and applied. On the application front, thin metal films of submicron thickness are typical examples of nanostructures that are widely used in modern high-speed electronic and opto-electronic devices. It is therefore important to develop a better understanding of electron transport and energy relaxation in the femtosecond temporal regime.

From a more fundamental point of view, the electron dynamics in a metallic nanostructure displays a broad range of physical regimes associated with various time scales. The following typical scenario is generally assumed. First, the electrons absorb quasi-instantaneously the laser energy via interband and/or intraband transitions. Under certain conditions (e.g. not too high energy transfer [6]) this early stage leads to the creation of a collective oscillation, the so-called surface plasmon. Subsequently, the plasmon oscillation is damped through coupling to self-consistent quasi-particle excitations (Landau damping) [7, 8]. This damping, which occurs on a very fast time scale ($\sim$10–50 fs), was observed experimentally in gold nanoparticles [9] and was studied theoretically in several works [8, 10, 11]. During these fast processes, the ionic background remains frozen and the electron distribution is nonthermal. As a result, the electron temperature cannot be properly defined at this stage of the relaxation process. On a longer timescale ($>$50 fs), the injected energy is redistributed among the electrons via electron–electron collisions, leading to the so-called 'internal' electron thermalization. Electron–lattice ('external') thermalization occurs on even longer time scales, of the order of a picosecond.

In the present work, we focus on the ultrafast electron dynamics in thin metallic films. Several experiments have shown [1, 2] that heat transport through the film involves ballistic

electrons traveling at the Fermi velocity of the metal. These findings were recently corroborated by accurate numerical simulations [12]–[14] obtained with a classical phase-space model (Vlasov–Poisson (VP) equations). These simulations also highlighted a regime of slow oscillations—corresponding to ballistic electrons bouncing back and forth on the film surfaces—whose period scales linearly with the thickness of the film. Such oscillations were recently measured in transient reflection experiments on thin gold films [15], and their period was shown to obey the predicted scaling.

The above results relied on a completely classical description of the electron dynamics, based on the evolution of a phase-space probability density according to the Vlasov equation [16]. Electron–electron interactions were taken into account within the mean-field approximation, via the electrostatic Poisson's equation (some attempts to include dynamical correlations beyond the mean field were also made). Despite its apparent simplicity, this model was able to predict observable results [15]: it must therefore contain the key elements of the physical phenomena at play in this type of experiment.

The purpose of the present work is to extend the past results to include quantum-mechanical effects. The quantum electron dynamics is governed by the Wigner equation coupled self-consistently to Poisson's equation. The Wigner representation [17] is a useful tool to express quantum mechanics in a phase-space formalism. In this representation, a quantum state (either pure or mixed) is described by a Wigner function, i.e. a function of the phase-space variables. Although the Wigner function satisfies most of the standard properties of probability distributions, it cannot be regarded as such, since it may take negative values. The Wigner–Poisson (WP) system can thus be considered as the most natural quantum–mechanical extension of the VP system, to which it reduces in the classical limit.

Here, we focus our attention on the electron dynamics in alkali metals (particularly sodium), for which the valence electrons are fully delocalized and the influence of the core electrons can be neglected. Simple sodium films constitute the first and simplest step toward more complex materials and, for this reason, should be thoroughly understood.

The time-dependent VP and WP equations are solved numerically using a grid-based method in the phase space [18], which does not rely on discrete particles and thus displays a very low level of numerical noise. Systematic comparisons between the classical and the quantum results will reveal a clear classical–quantum transition occurring at low excitation energies.

In the rest of this paper, we express all quantities in terms of the following normalized units. Time is normalized to the inverse of the plasmon frequency $\omega_p = (e^2\bar{n}_i/m\varepsilon_0)^{1/2}$, where m and $e > 0$ are the electron mass and absolute charge, respectively, and ε_0 is the dielectric constant in vacuum. Velocities are normalized to the Fermi speed v_F and distances to the Thomas–Fermi screening length $L_F = v_F/\omega_p$. In addition, particle densities are normalized to the ion density of the bulk metal $\bar{n}_i$. Table 1 summarizes the principal physical parameters for the typical cases of sodium and gold films, which are frequently used in experiments.

2. Ground state

Following the same approach adopted in our previous works [12]–[14], the study of the electron dynamics can be divided into two steps: (i) first, the ground state of the electron population (at finite temperature) is determined self-consistently; and (ii) subsequently, the ground state is

Table 1. Typical parameters for gold and sodium films.

	Units	Au	Na
$\bar{n}_i$	m^{-3}	5.9×10^{28}	2.5×10^{28}
ω_p^{-1}	fs	0.07	0.11
$\hbar\omega_p$	eV	9.02	5.87
E_F	eV	5.53	3.12
T_F	K	6.41×10^4	3.62×10^4
L_F	nm	0.09	0.12
v_F	$m\,s^{-1}$	1.39×10^6	1.05×10^6
r_s	nm	0.16	0.21
r_s/a_0	–	3.01	4.0

perturbed by injecting some energy into the system, generally in the form of kinetic energy of the center-of-mass. The ensuing dynamics is then followed for a certain duration.

For the quantum case, the dynamics is described by the time-dependent Wigner equation, which, as mentioned earlier, is the natural quantum generalization of the Vlasov equation [17]. However, the Wigner approach is intrinsically ill-suited to deal with stationary states (indeed, quantization rules are overlooked by the Wigner formalism, and must be imposed as additional constraints). It is more convenient to determine the ground state from a standard density-functional approach (Kohn–Sham equations), and then construct the Wigner function from the computed Kohn–Sham wavefunctions.

Throughout this work, we assume that the film size in the directions parallel to its surfaces is large compared with its thickness L. In this case, the electron motion parallel to the surface is completely decoupled from the motion normal to the surface, and a one-dimensional (1D) model can be adopted.

The electron gas is assumed to be at thermal equilibrium with temperature T_e. In the Kohn–Sham formulation of the density-functional theory, the ground-state electron density n_e can be written as

$$n_e(x) = \sum_{k=1}^{\infty} p_k \, |\varphi_k(x)|^2, \tag{1}$$

where φ_k and ε_k are the single-particle orbitals and energies, respectively, and

$$p_k = \frac{m}{\pi\hbar^2\beta} \ln\left[1 + e^{\beta(\varepsilon_k - \mu)} - \beta(\varepsilon_k - \mu)\right] \tag{2}$$

are the occupation numbers corresponding to a Fermi–Dirac distribution after integration over the energy coordinates parallel to the film surface. Here, μ is the chemical potential and $\beta = 1/k_B T_e$. These orbitals and energies obey the 1D Schrödinger equation

$$\left[-\frac{\hbar^2}{2m}\frac{\partial^2}{\partial x^2} + V_{\text{eff}}(x)\right]\varphi_k(x) = \varepsilon_k \varphi_k(x), \tag{3}$$

where the effective potential $V_{\text{eff}}(x) = V_H(x) + V_{xc}(x)$ is composed of a Hartree part V_H and an exchange–correlation part $V_{xc}[n_e(x)]$. The Hartree potential also includes the effect of the ions,

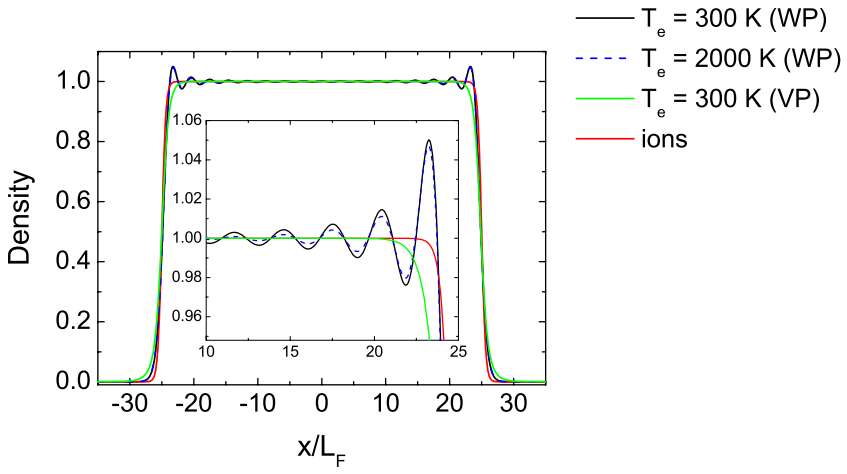

Figure 1. Ground-state electron and ion densities, for a film with $L = 50L_F$, $\sigma_i = 0.3L_F$ and different electron temperatures, in the classical regime (VP) and in the quantum regime (WP). The inset shows a zoom near the film surface.

and obeys Poisson's equation:

$$\frac{d^2V_H}{dx^2} = \frac{e}{\varepsilon_0}[n_e(x) - n_i(x)]. \tag{4}$$

In the framework of the jellium model, the ions are described by a continuous, immobile density with soft edges, $n_i(x) = \bar{n}_i\{1 + \exp[(|x| - L/2)/\sigma_i]\}^{-1}$, where $\bar{n}_i = 3/(4\pi r_s^3)$ is the ion density of the bulk metal, r_s is the Wigner–Seitz radius, and σ_i is a diffuseness parameter. Typical parameters used in the simulations are as follows: film thickness $L = 50L_F$ (≈ 6 nm for sodium films), diffuseness parameter $\sigma_i = 0.3L_F$, and electron temperature in the range $T_e = 0$–2000 K.

Except where otherwise stated, we will neglect the exchange–correlation potential, so that the Kohn–Sham equations (3) reduce to the Hartree (mean-field) equations. This will facilitate the comparison with the classical VP results, for which only the Hartree potential was present. A few runs will be performed with exchange and correlations, in order to show that the results are not sensitive to this effect and do not depend on the specific form of V_{xc}. To this purpose, we shall use the functionals suggested by Brey *et al* [19].

The Kohn–Sham equations (3) are solved numerically using a finite-difference iterative method [20]. The number of occupied states is $N = 18$ for a film with $L = 50L_F$ and $T_e = 0$; more states are occupied at finite temperature. Some typical density profiles at various electron temperatures are shown in figure 1. The classical VP result yields a smooth density profile (without oscillations). In the quantum regime (labeled WP), the standard Friedel oscillations are observed, particularly near the film surface. Note that the profiles are weakly dependent on the electron temperature.

After computing the N Kohn–Sham wavefunctions φ_k and the respective occupation numbers p_k, we can proceed to construct the ground-state Wigner function $f(x, v)$. We first compute the partial Wigner functions corresponding to each Kohn–Sham wavefunction of the ground state:

$$f_k(x, v) = \frac{m}{2\pi\hbar}\int_{-\infty}^{+\infty} \varphi_k^*\left(x + \frac{\lambda}{2}, t\right)\varphi_k\left(x - \frac{\lambda}{2}, t\right)e^{imv\lambda/\hbar}d\lambda. \tag{5}$$

The total Wigner function is then the sum of the partial Wigner functions, weighted with the occupation numbers p_k: $f(x, v) = \sum_{k=1}^{N} p_k f_k(x, v)$.

As an illustration, we show in figure 2 some typical ground-state Kohn–Sham wavefunctions and the corresponding partial Wigner functions, for a film of thickness $L = 50L_F$. The total Wigner function is shown in figure 3.

3. Dynamics

3.1. Model

To study the electron dynamics, we make use of the evolution equation for the Wigner function. It is an integro-differential equation that reads as:

$$\frac{\partial f}{\partial t} + v\frac{\partial f}{\partial x} + \mathrm{i}\frac{em}{2\pi\hbar^2}\int \mathrm{d}\lambda\, \mathrm{d}v' \mathrm{e}^{\mathrm{i}m(v-v')\lambda/\hbar}\left[V_{\mathrm{eff}}\left(x+\frac{\lambda}{2}, t\right)\right.$$
$$\left. - V_{\mathrm{eff}}\left(x-\frac{\lambda}{2}, t\right)\right] f(x, v', t) = 0, \tag{6}$$

where $V_{\mathrm{eff}}(x, t)$ is composed of a Hartree and an exchange–correlation part. For the latter, we employ the adiabatic local-density approximation (ALDA), i.e. we use the same functional as in the ground-state calculation [19], but allow for a time dependence of the electron density. The Hartree potential obeys Poisson's equation

$$\frac{\partial^2 V_{\mathrm{H}}}{\partial x^2} = \frac{e}{\varepsilon_0}\left(\int f \mathrm{d}v - n_{\mathrm{i}}(x)\right). \tag{7}$$

In the classical limit (i.e. taking $\hbar \to 0$ and neglecting exchange and correlations), equation (6) reduces to the Vlasov equation that was used in our previous works [12]–[14].

The boundary conditions are as follows: for the electron distribution, we define a computational box $-L_{\max}/2 \leqslant x \leqslant L_{\max}/2$ and $-v_{\max} \leqslant v \leqslant v_{\max}$, with $L_{\max} \gg L$ (the thickness of the film) and $v_{\max} \gg v_F$. The Poisson's equation is solved with boundary conditions $V_{\mathrm{H}}(-L_{\max}/2) = V_{\mathrm{H}}(L_{\max}/2) = 0$. The results were obtained with a numerical code based on a uniform grid covering the relevant phase space [18]. The method combines the split-operator technique with fast Fourier transforms in the velocity coordinate.

In order to excite the electron dynamics, one has to perturb the initial ground-state equilibrium. This is done by imparting a uniform velocity shift δv to the initial distribution. Thus, some energy is injected into the electron gas in the form of kinetic energy of the center-of-mass.

Previous classical studies had yielded the following scenario [12]–[14]: (i) during an initial stage of the evolution, the center-of-mass energy is quickly converted into thermal energy, thus increasing the temperature of the electron gas; (ii) for longer times, slow nonlinear oscillations appear, with a period proportional to the thickness of the film. These oscillations were attributed to nonequilibrium electrons bouncing back and forth on the film surfaces. Indeed, phase-space portraits of the electron distribution showed bunches of electrons traveling at the Fermi velocity, colliding with one of the surfaces, and eventually being reflected backwards (see also section 3.3).

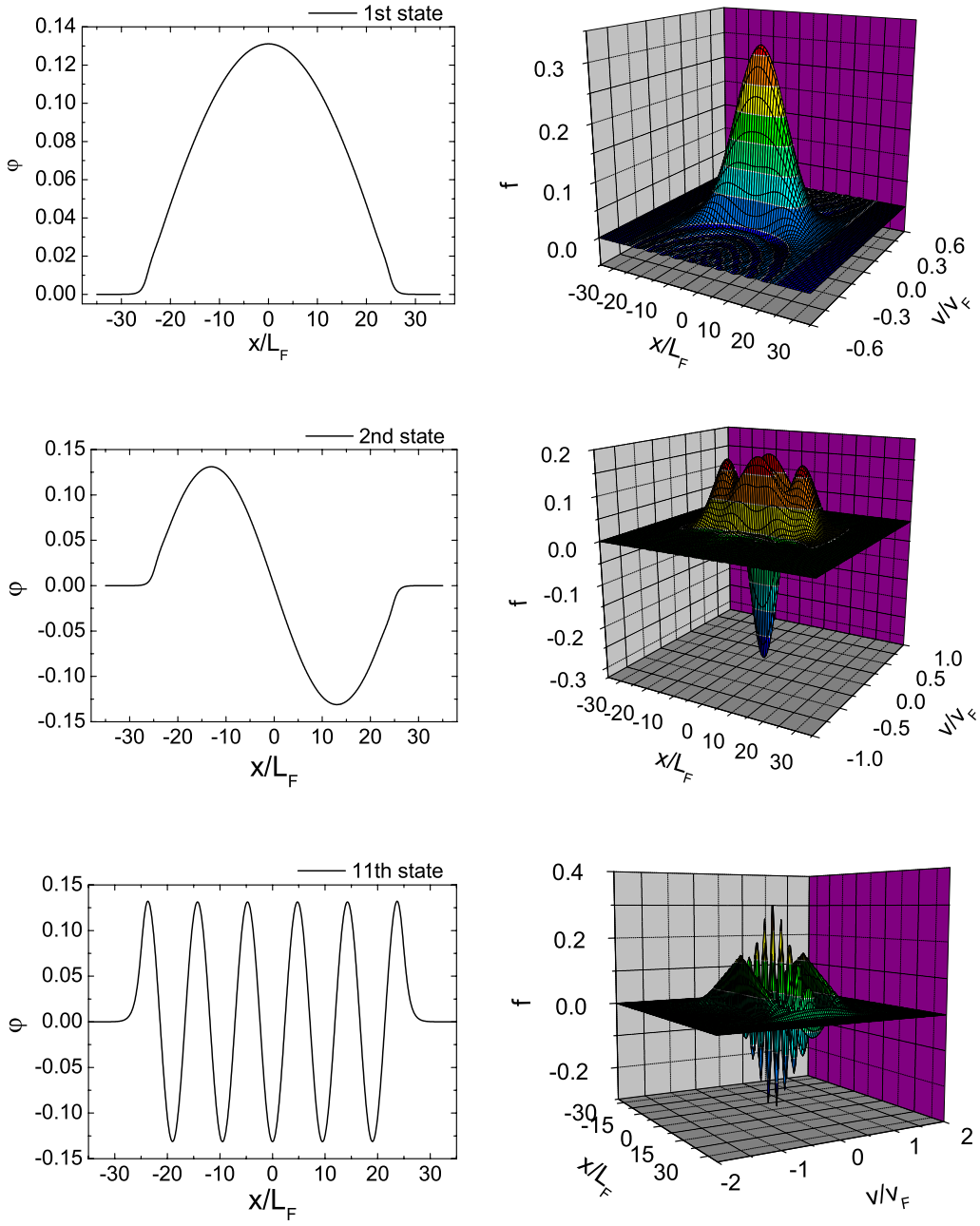

Figure 2. Kohn–Sham wavefunctions (left column) and corresponding partial Wigner functions (right column) for the 1st state (top frames), 2nd state (middle frames), and 11th state (bottom frames), for a typical film with $L = 50L_{\mathrm{F}}$, $\sigma_{\mathrm{i}} = 0.3L_{\mathrm{F}}$ and $T_{\mathrm{e}} = 300\,\mathrm{K}$.

In the present work, our main purpose is to ascertain to what extent the classical results remain valid in the fully quantum regime. We are particularly interested in the behavior of the low-frequency oscillations, which were observed experimentally [15] and could provide a useful check for the transition between the classical and the quantum regimes. Our main control

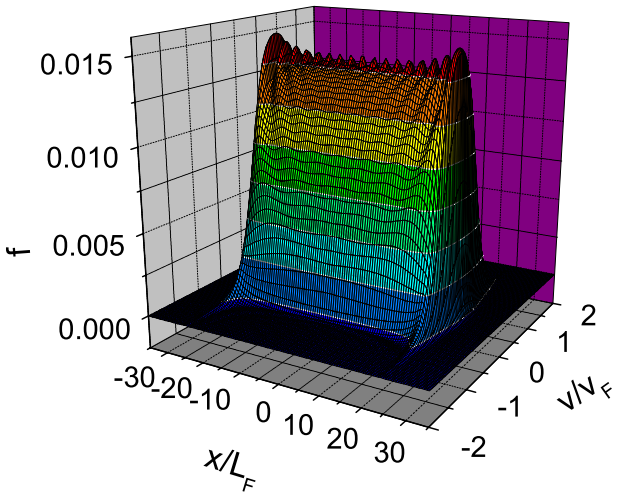

Figure 3. Total Wigner function for a typical film with $L = 50L_F$, $\sigma_i = 0.3L_F$ and $T_e = 300\,K$.

parameter will be the strength of the initial perturbation δv. *A priori*, it is reasonable to expect that quantum effects should play a role mainly in the regime of weak perturbations.

3.2. Low-frequency oscillations

Several energy quantities were considered (all normalized to the Fermi energy). The total energy of the electron gas is given by the sum of kinetic plus potential energy: $E_{tot} = E_{kin} + E_{pot}$. Further, the kinetic energy can be split into three parts: the energy of the center-of-mass $E_{cm} = \frac{1}{2}\int \frac{j_e^2}{n_e}\,dx$ (where $j_e = \int vf\,dv$ is the electron current), the Thomas–Fermi energy (energy of the equivalent zero-temperature state with the same density) $E_{TF} = \frac{1}{5}\int n_e(x)^{5/3}dx$ and the thermal energy, $E_{th} = E_{kin} - E_{TF} - E_{cm}$. The thermal energy corresponds to the kinetic energy of the electrons located in a shell of thickness $k_B T_e$ around the Fermi surface.

In figure 4, we plot the evolution of the thermal and centre-of-mass energies for the Vlasov and Wigner simulations, in the case of a strong perturbation, $\delta v = 0.15 v_F$, for a typical sodium film with $L = 50L_F$ and $T_e = 300\,K$. The general behaviour of these quantities is roughly similar in both the classical and quantum cases. An initial phase of the dynamics features fast collective oscillations of the centre-of-mass at the plasma frequency. During this phase, the centre-of-mass energy is rapidly damped (Landau damping) and converted into thermal energy. After saturation of the thermal energy at $\omega_p t \simeq 200$, a slowly oscillating regime appears. Classically, the period T of these slow oscillations is roughly equal to the time of flight of electrons traveling through the film at a velocity close to the Fermi speed of the metal, i.e. $T = L/v_F$ [12, 13]. In the quantum case, the measured period of the slow oscillations is basically the same, although the details of the evolution are obviously different.

A first difference between the classical and quantum evolutions is that the centre-of-mass energy does not completely decay to zero in the quantum regime. This effect was already observed in quantum hydrodynamic simulations [21] and implies that Landau damping (i.e., the coupling of the centre-of-mass coordinates to the internal degrees of freedom of the electron gas) is acting less efficiently in the quantum regime. Indeed, Landau damping

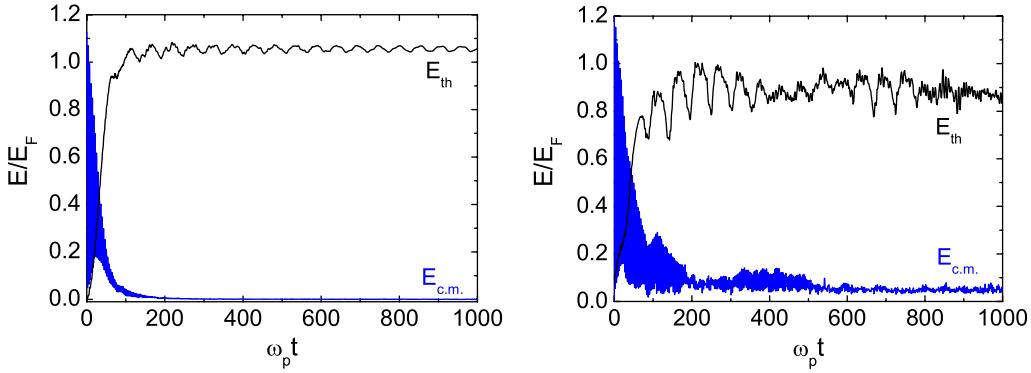

Figure 4. Time evolution of the thermal and centre-of-mass energies in the classical case (left panel) and quantum Hartree case (right panel), for $T_e = 300$ K, $L = 50L_F$ and $\delta v = 0.15v_F$.

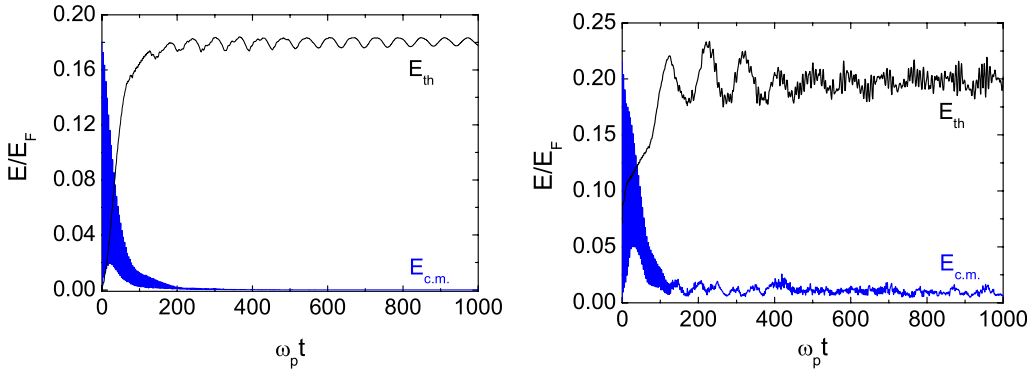

Figure 5. Same as figure 4 but for $\delta v = 0.06v_F$.

is a phase-mixing effect that arises from many different states oscillating at slightly different frequencies and is thus amplified in the classical regime, where the number of states is effectively infinite. When the spectrum is discrete and the number of states is finite, beatings and revivals can occur, thus reducing the efficiency of Landau damping. Indeed, a revival is visible in figure 4 (right panel) around $\omega_p t \simeq 400$, with an increase of the centre-of-mass energy and the corresponding decrease of the thermal energy.

Let us now return to the slow nonlinear oscillations. By reducing the magnitude of the perturbation to $\delta v = 0.06v_F$, we still observe some low-frequency oscillations in the quantum dynamics (right panel of figure 5). However, their period is significantly longer than that of the corresponding Vlasov results (left panel of figure 5). Clearly, some new effect is kicking in at low excitations, which alters the simple picture of electron bunches traveling through the film at the Fermi velocity.

In order to understand this point, in figure 6 we plot the observed period T of the low-frequency oscillations against the value of the perturbation. As expected, the classical and quantum results coincide for large excitations (i.e. the period is close to the ballistic value $T = L/v_F$), but they start to diverge near a certain threshold δv_{th}. Below the threshold, the period stays close to the ballistic value for the Vlasov simulations, whereas it becomes considerably larger for the Wigner results.

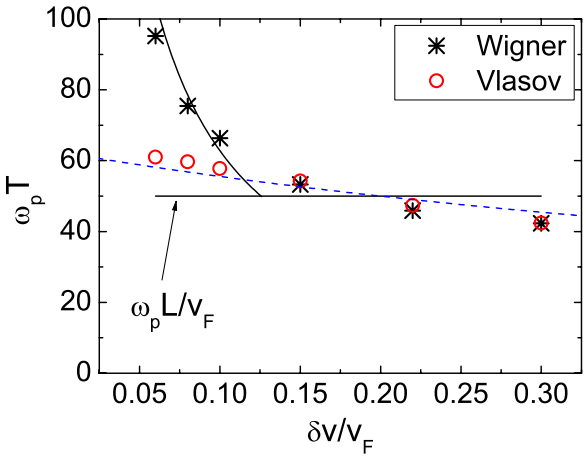

Figure 6. Period of the low-frequency electron oscillations as a function of the perturbation, for a slab of thickness $L = 50L_F$ and temperature $T_e = 300\,K$, in the classical (Vlasov) and quantum (Wigner) regimes. The quantum results neglect exchange and correlations (Hartree model). The horizontal solid line corresponds to the ballistic period L/v_F; the solid curve at small excitations refers to equation (9) and the dashed line corresponds to the corrected period $T = L/(0.8v_F + |\delta v|)$.

Thus, we observe a clear transition between a classical and a quantum regime occurring at a fairly well-defined threshold. To estimate the value of this threshold, we must go back to the VP results published in our previous works [12]–[14]. There, it was shown that bunches of nonequilibrium electrons travel at a velocity close to v_F between the surfaces of the film. These bunches (i.e. vortices in the phase space) have a spatial extension roughly equal to $2\pi L_F$ and a width of the order of δv in velocity space (see also figure 11 in section 3.3). The phase-space surface of these vortices (which has the dimension of an action) is thus approximately $S \simeq 2\pi L_F m\delta v$. We expect that quantum effects become significant when this action is of the same order as Planck's constant, i.e. $S \approx \hbar$. This leads to the following expression for the threshold, in dimensionless units:

$$\frac{\delta v_{th}}{v_F} = \frac{\hbar\omega_p}{4\pi E_F}. \tag{8}$$

For sodium films, this yields $\delta v_{th} \approx 0.15 v_F$, which is fairly close to the observed value.

The same threshold can be interpreted from a different angle. The perturbation δv slightly changes the velocity of the electrons lying near the Fermi surface. For these electrons, the change in kinetic energy can be written as $\delta E = m v_F \delta v$. Using equation (8), we obtain that the threshold can be expressed as $\delta E_{th} = \hbar\omega_p/2\pi$. Thus, quantum effects become important when the excitation induces a change in the kinetic energy on the Fermi surface that is significantly smaller than the plasmon energy $\hbar\omega_p$.

Below the threshold, the quantum results still display some persistent low-frequency oscillations, but these are no longer related to the ballistic motion of the electrons and subsequent bouncing on the surfaces. Instead, the quantum oscillations can be linked to the

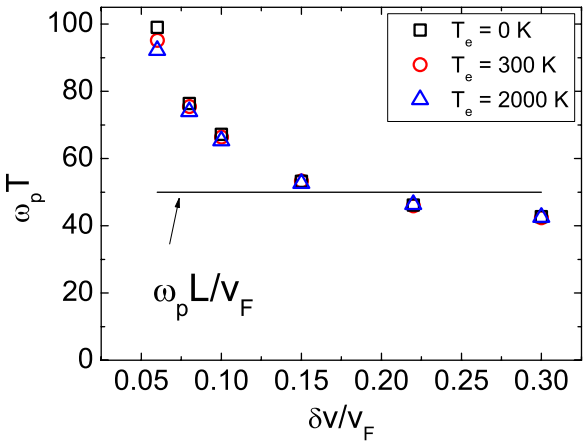

Figure 7. Period of the low-frequency oscillations as a function of the perturbation, for a slab of thickness $L = 50L_{\mathrm{F}}$ and various electron temperatures in the range $T_{\mathrm{e}} = 0$–$2000\,\mathrm{K}$. Quantum (Wigner) regime without exchange and correlations.

excitation energy around the Fermi surface in such a way that $\hbar\omega = \delta E$, where $\omega = 2\pi/T$ is the oscillation frequency. Then, we obtain for the period:

$$T = \frac{2\pi\hbar}{m v_{\mathrm{F}} \delta v}, \tag{9}$$

which is the curve depicted in figure 6. Despite the simplicity of the above argument, equation (9) reproduces rather well the observed data. All in all, the oscillations observed in the small-perturbation regime appear to be linked to the excitation of quantum eigenmodes close to the Fermi level. In contrast, for large perturbations, many states are excited simultaneously, thus triggering the classical ballistic regime at the Fermi speed.

Going back to the Vlasov results in figure 6, we note that the period displays a weak dependence on the perturbation amplitude, which is not accounted for by the ballistic expression $T = L/v_{\mathrm{F}}$. This can be explained as follows. Firstly, it was already noted in previous works [13] that the transit velocity of the electrons is slightly smaller than the Fermi speed, say $\approx 0.8 v_{\mathrm{F}}$. Secondly, the actual transit velocity should also include the perturbation δv. Including these effects, the oscillation period should be $T \approx L/(0.8 v_{\mathrm{F}} + |\delta v|)$, which corresponds to the dashed line in figure 6 and appears to agree rather well with the Vlasov results all over the perturbation range.

The effect of the electron temperature is investigated in figure 7 with the Wigner model. For all the cases shown here, the quantum–classical transition is still clearly observed at small perturbations. All in all, the oscillation period depends very weakly on the electron temperature.

Finally, in figure 8 we show the effect of exchange and correlations on the period of the slow oscillations. The observed period is slightly smaller (compared with the Hartree result) in the low-excitation regime, whereas it converges again to the Vlasov results for high excitations. As the combined effect of exchange and correlations has a considerable impact on the ground-state potential, it is not too surprising that the oscillation period is also affected.

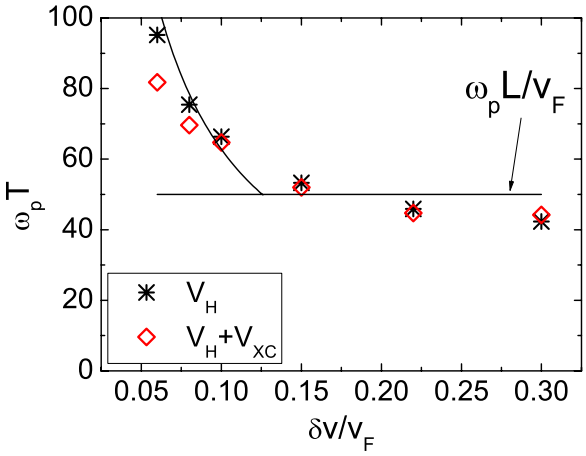

Figure 8. Period of the low-frequency oscillations as a function of the perturbation, for a slab of thickness $L = 50L_F$ and temperature $T_e = 300\,K$, in the quantum (Wigner) regime. Black stars: purely Hartree model; red diamonds: Hartree plus exchange and correlations.

Nevertheless, a clear departure from the ballistic value of the period is still observed for low excitations.

3.3. Phase-space dynamics

In our previous works on the classical Vlasov model [12]–[14], it was clearly shown that the oscillations studied in the above paragraphs are due to electrons traveling through the film at a velocity close to the Fermi speed of the metal. Indeed, the phase-space portraits of the electron distribution function revealed the presence of traveling vortices around $v = v_F$. We have already discussed the fact that the transition between the classical and quantum behavior occurs when the size of these vortices becomes of the order of Planck's constant.

The Wigner approach is particularly useful for directly comparing the quantum and classical phase-space portraits. These are shown in figures 9 and 10, for high and low excitation amplitudes, respectively. For the larger excitation ($\delta v = 0.15 v_F$, figure 9), both the Vlasov and the Wigner simulations feature several coherent structures (vortices) propagating ballistically at the Fermi velocity. For the smaller excitation value ($\delta v = 0.06 v_F$, figure 10), the vortices are still visible in the Vlasov regime, but they have completely disappeared from the Wigner simulations. In this case, the Vlasov and Wigner regimes exhibit clearly different properties in their respective phase-space portraits. Four movies available from stacks.iop.org/NJP/11/063042/mmedia—with excitation amplitudes $\delta v/v_F = 0.06$, 0.08, 0.15 and 0.25—illustrate the difference between the Vlasov and Wigner dynamics in the phase space.

A zoom on the phase-space portraits (figure 11) confirms the presence of electron vortices near the Fermi speed. Quantum effects can destroy these vortices, thus preventing the ballistic oscillations occuring. In this specific case $\delta v = 0.06 v_F$, so that the area (action) of a phase-space vortex is, in normalized units, $S/(m v_F L_F) \approx 2\pi \delta v/v_F = 0.38$. This is smaller than the normalized Planck's constant $\hbar/(m v_F L_F) \approx 0.94$ for sodium, so that quantum effects are indeed strong enough to hinder the formation of the vortices.

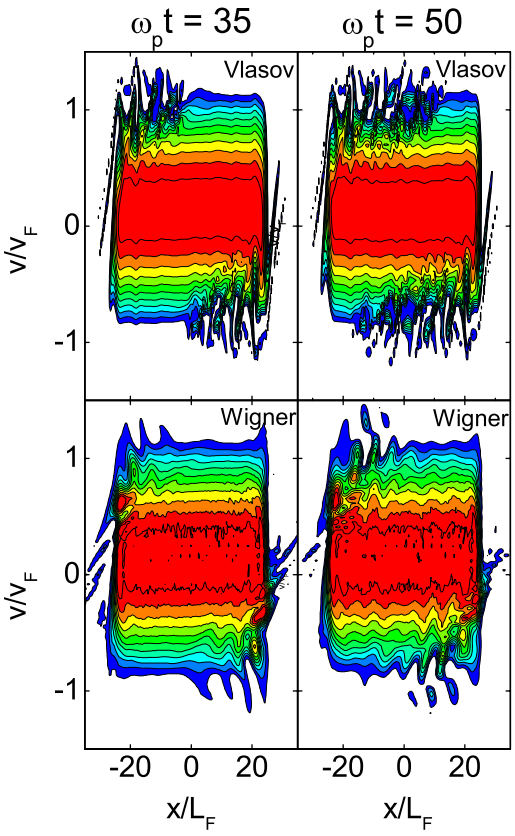

Figure 9. Contour plots of the electron distribution function in the phase space at different instants, $\omega_p t = 35$ (left panels) and $\omega_p t = 50$ (right panels), for a large excitation $\delta v = 0.15 v_F$. Top panels: classical results and bottom panels: quantum results.

4. Conclusion

In this work, we extended previous studies on the electron dynamics in thin metal films, by including quantum-mechanical effects through the Wigner phase-space representation.

Previous (purely classical) simulations had highlighted a regime of low-frequency 'ballistic' oscillations due to the bouncing of nonequilibrium electrons on the film surfaces [12, 13]. These oscillations were subsequently observed in experiments on thin gold films [15].

The purpose of the present work was to investigate the impact of quantum effects on the electron dynamics. Our key result was that, by reducing the strength of the initial excitation, a neat transition from a classical to a quantum regime could be observed. Indeed, at weak excitation energies (smaller than one quantum of plasmon energy, $\hbar\omega_p$) the period of the low-frequency oscillations departs significantly from the ballistic value observed in the classical simulations. The estimated threshold of this quantum–classical transition agrees well with the simulations. We also proved that this result is robust, in the sense that it depends only weakly on physical parameters such as the electron temperature, or the choice of a specific exchange–correlation functional.

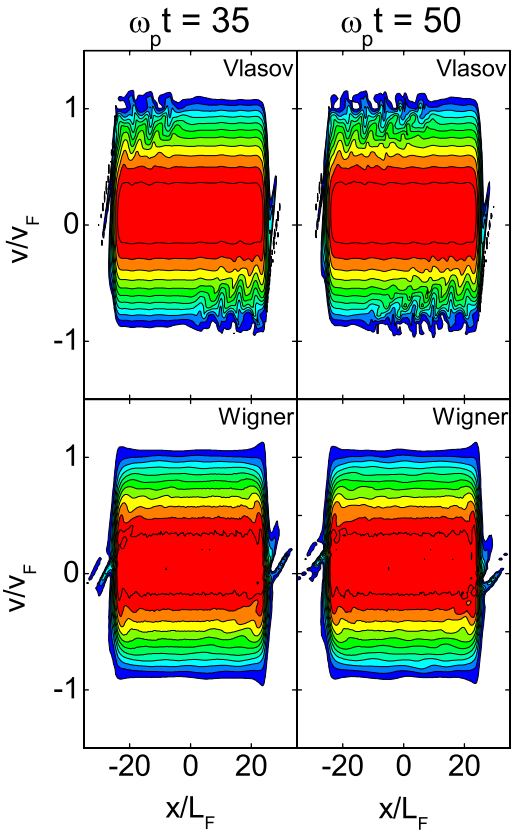

Figure 10. Same as figure 9 but for a weaker excitation, $\delta v = 0.06 v_{\mathrm{F}}$.

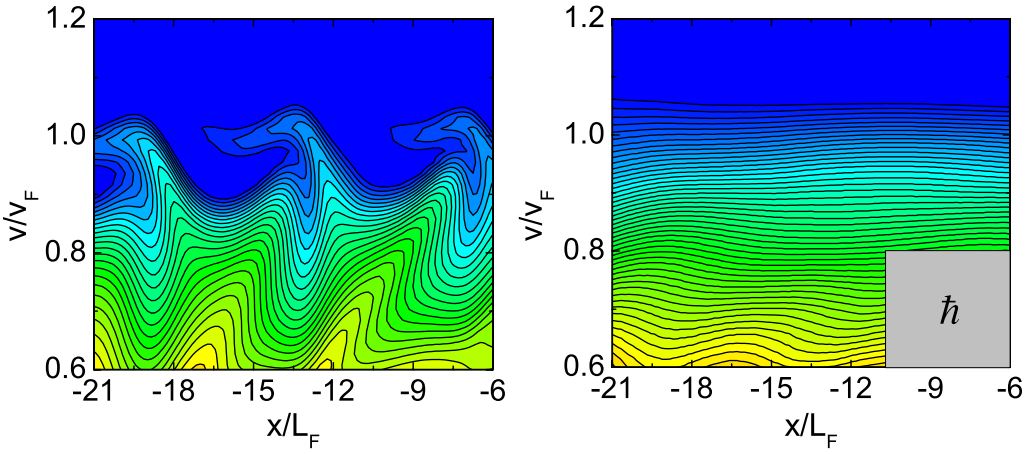

Figure 11. Zoom of the electron distribution function in the phase-space region near the Fermi surface, at time $\omega_{\mathrm{p}} t = 35$, for a film of thickness $L = 50 L_{\mathrm{F}}$, temperature $T_{\mathrm{e}} = 300\,\mathrm{K}$, and excitation $\delta v = 0.06 v_{\mathrm{F}}$. Vortices are present in the Vlasov phase-space portrait (left panel), but not in the Wigner one (right panel). The shaded area in the right panel represents Planck's constant in normalized units, i.e. $\hbar/(m v_{\mathrm{F}} L_{\mathrm{F}})$.

The above findings constitute an example of a quantum–classical transition in the electron dynamics that could, in principle, be observed experimentally. For instance, in a previous work [14] we showed that the ballistic oscillations could be used to enhance the energy absorption by the electron gas, when the film is irradiated with an electromagnetic wave (laser pulse) that matches the frequency of the ballistic oscillations (for sodium films, the frequency lies in the infrared range). This is a case of nonlinear resonant absorption. In the quantum regime, the resonant frequency should be further redshifted (because the period increases), and the overall effect could be observable experimentally.

Further, recent pump–probe experiments [22] carried out on single metal nanoparticles (whose size is therefore well controlled) revealed an increase of the expected electron–phonon relaxation time when the particle's diameter is less than 2 nm. This anomalous behavior was attributed to quantum effects arising from the discrete nature of the electronic states inside such small nanoparticles.

In our simulations, the quantum–classical transition occurs not by reducing the size, but by weakening the external excitation. This might make it even easier to observe in practice, as a precise knowledge of the film thickness is not *a priori* required. In addition, although our approach pertains primarily to alkali metals (particularly sodium), the observed effects should be generic and have a wider application to noble-metal films (Au and Ag), which are generally used in the experiments.

References

[1] Brorson S D, Fujimoto J G and Ippen E P 1987 *Phys. Rev. Lett.* **59** 1962
[2] Suárez C, Bron W E and Juhasz T 1995 *Phys. Rev. Lett.* **75** 4536
[3] Sun C-K, Vallée F, Acioli L H, Ippen E P and Fujimoto J G 1994 *Phys. Rev.* B **50** 15337
[4] Bigot J-Y, Halté V, Merle J-C and Daunois A 2000 *Chem. Phys.* **251** 181
[5] Voisin C, Christofilos D, Del Fatti N, Vallée F, Prével B, Cottancin E, Lermé J, Pellarin M and Broyer M 2000 *Phys. Rev. Lett.* **85** 2200
[6] Madjet M and Hervieux P-A 1999 *Eur. Phys. J.* D **9** 217
[7] Kawabata A and Kubo R 1966 *J. Phys. Soc. Japan* **21** 1765
[8] Kreibig U and Vollmer M 1995 *Optical Properties of Metal Clusters* (New York: Springer)
[9] Lamprecht B, Krenn J R, Leitner A and Aussenegg F R 1999 *Phys. Rev. Lett.* **83** 4421
[10] Molina R A, Weinmann D and Jalabert R A 2002 *Phys. Rev.* B **65** 155427
[11] Zaretsky D F, Korneev Ph A, Popruzhenko S V and Becker W 2004 *J. Phys. B: At. Mol. Opt. Phys.* **37** 4817
[12] Manfredi G and Hervieux P-A 2004 *Phys. Rev.* B **70** 201402
[13] Manfredi G and Hervieux P-A 2005 *Phys. Rev.* B **72** 155421
[14] Manfredi G and Hervieux P-A 2005 *Opt. Lett.* **30** 3090
[15] Liu X, Stock R and Rudolph W 2005 *Phys. Rev.* B **72** 195431
[16] Calvayrac F, Reinhard P-G, Suraud E and Ullrich C 2000 *Phys. Rep.* **337** 493
[17] Hillery M, O'Connell R F, Scully M O and Wigner E P 1984 *Phys. Rep.* **106** 121
[18] Suh N, Feix M R and Bertrand P 1991 *J. Comput. Phys.* **94** 403
[19] Brey L, Dempsey J, Johnson N F and Halperin B I 1990 *Phys. Rev.* B **42** 1240
[20] Eguiluz A G 1984 *Phys. Rev.* B **30** 5449
[21] Crouseilles N, Manfredi G and Hervieux P-A 2008 *Phys. Rev.* B **78** 155412
[22] Arbouet A *et al* 2003 *Phys. Rev. Lett.* **90** 177401